Non-Hermitian $\mathcal{CT}$-Symmetric Spectral Protection of Nonlinear Defect Modes

Do Hyeok Jeon,[1] Mattis Reisner,[2] Fabrice Mortessagne,[2,*] Tsampikos Kottos,[1,†] and Ulrich Kuhl[2,‡]
[1]Wave Transport in Complex Systems Lab, Physics Department, Wesleyan University, Middletown, Connecticut 06459, USA
[2]Université Côte d'Azur, CNRS, Institut de Physique de Nice (INPHYNI), Nice 06108, France

(Received 16 February 2020; accepted 18 August 2020; published 9 September 2020)

We investigate, using a microwave platform consisting of a non-Hermitian Su-Schrieffer-Heeger array of coupled dielectric resonators, the interplay of a lossy nonlinearity and $\mathcal{CT}$ symmetry in the formation of defect modes. The measurements agree with the theory which predicts that, up to moderate pumping, the defect mode is an eigenstate of the $\mathcal{CT}$-symmetric operator and retains its frequency at the center of the gap. At higher pumping values, the system undergoes a self-induced explicit $\mathcal{CT}$-symmetry violation which removes the spectral topological protection and alters the shape of the defect mode.

DOI: 10.1103/PhysRevLett.125.113901

Introduction.—Topological photonics (TP) [1,2] has originally developed within the framework of Hermitian wave physics, drawing inspirations from the discovery of exotic topological phases appearing in traditional condensed matter. Its rapid blossom relies on the promise that the developed TP methodologies, based on geometrical and topological concepts, can lead to unprecedented control on light-matter interactions. A prominent application is the realization of photonic structures with transport characteristics that are immune to fabrication imperfections [3–6]. Most of these investigations principally focus on linear topological phenomena. Recently, however, it has been realized that nonlinearities, when invoked, can offer a dynamical tuning mechanism that produces various exotic phenomena. Examples include robust discrete solitons [7], self-localized topological edge solitons [8,9], topologically enhanced harmonic generation [10], optical isolation [11], topological lasers [12], and self-induced topological states [13–15].

The topological physics agenda (set initially by the condensed matter community) has been enlarged and redefined by the necessities presented in the optics framework. In particular, the natural presence of non-Hermitian elements like gain and loss "demands" the redefinition or (even) invention of new topological concepts and classifications. The interplay between non-Hermiticity and topological protection attracted recently a lot of theoretical and experimental interest [16–33]. Questions raised are the generalization of band edge correspondence, the emergence of new topological states without any Hermitian counterpart, or the necessity of a new topological phase classification [2,25,29,31]. On the technological side, the development of novel classes of topologically protected lasers [26–28] and reflective photonic limiters [22,32,33] introduced a new excitement and the urge to understand better the formation and spectral stability of topological states in the framework of non-Hermitian physics.

Here we analyze, both experimentally and theoretically, the intricate effects that nonlinearity together with non-Hermiticity have in the formation of a topological defect mode. Our platform utilizes a standard Su-Schrieffer-Heeger (SSH) binary array consisting of identical microwave resonators coupled electromagnetically with one another. In the middle of the array we position one defect resonator which involves both linear and nonlinear losses, thus enforcing a charge-conjugation ($\mathcal{CT}$) symmetry to the whole SSH structure. We find that the emerging defect mode is an eigenmode of the $\mathcal{CT}$ operator. Furthermore, under pump-probe measurements, this mode is resilient to a large range of pumping powers, with its frequency being pinned at the center of the band gap. For higher values of the pump, the system experiences a self-induced explicit $\mathcal{CT}$-symmetry violation that enforces the destruction of the defect mode. The measurements are in agreement with the results from a theoretical analysis which utilizes a modified non-Hermitian Green's function's formalism that treats the non-Hermitian nonlinear defect perturbatively. Our results paves the way for the design of topologically protected isolators, circulators, or switches with self-induced reconfigurability.

Modeling of SSH CROW array.—A simple platform to examine the interplay of nonlinearities with non-Hermiticity and topological protection is the SSH model [34]. It is a one-dimensional periodic array of identical resonators with alternating short (d_1) and long (d_2) distances from one another. A defect resonator is introduced in the middle of the chain, by separating two consequent resonators by long distances, and it supports linear and nonlinear losses. We have implemented experimentally this setup by a coupled resonator microwave waveguide (CRMW) array, see Fig. 1. The array consists of $N = 17$ high-index ($n_r = 6$) cylindrical resonators (radius $r = 4$ mm, height $h = 5$ mm) made of ceramics (ZrSnTiO) with resonant frequency around $\epsilon \approx 6.876$ GHz. The distances between the resonators is

FIG. 1. The experimental setup. Dielectric resonators are placed on an alumina plate and form an SSH structure, with intradimer distance $d_1 = 10$ mm (strong coupling $t_1 = 68$ MHz, indicated by braces). The interdimer distance is $d_2 = 12$ mm (weak coupling $t_2 = 33$ MHz). The central resonator ($m = 0$) is weakly coupled to both neighbors and on top of it the short circuited diode is seen on a teflon spacer. The kinked excitation antenna is positioned at the defect resonator. A top metallic plate supports the scanning loop antenna (not shown).

$d_1 = 10$ mm and $d_2 = 12$ mm corresponding to strong $t_1 = 68$ MHz and weak $t_2 = 33$ MHz electromagnetic coupling, respectively. We have incorporated the nonlinearity by coupling the central resonator with a diode (Schottky diode SMS7630-079LF from Skyworks) by placing it above the defect resonator using a Teflon spacer. The diode is short circuited and coupled via a metallic ring with a diameter of 3 mm. Thus the z-directional magnetic field at the defect resonator is inductively coupled to the fast diode. The system is pumped via a vector network analyzer (ZVA 24 from Rohde and Schwarz) which injects powers P_{VNA} ranging from -200 to 10 dBm via strongly coupled kink antennas (see Fig. 1). Note that this is not the real applied power on the defect resonator as there are additional absorption in the cables, the coupling of the antenna to the defect resonator, and other loss types, which are all of linear type. Instead, the field intensity at the defect resonator I_D is proportional to the injected power, $I_D = a_{\mathrm{lin}} P_{\mathrm{VNA}}$ in the steady state situation realized by the experiment. The field is probed by a weakly coupled loop antenna fixed on the top plate which is movable. For details on the antennas and the experimental setup, see [32].

The experimental setup is described mathematically within the framework of couple mode theory [35,36]. In our modeling we do not consider any linear dispersion effects which are negligible in the frequency range of our experiment. In the following, we use the Dirac notation:

$$\begin{aligned} \mathcal{H}|\Psi_l\rangle &= \omega_l|\Psi_l\rangle, \qquad |\Psi_l\rangle = \sum_m \psi_m^{(l)}|m\rangle, \\ \mathcal{H} &= \sum_m |m\rangle\epsilon_m\langle m| + |m\rangle t_{m,m-1}\langle m-1| \\ &\quad + |m\rangle t_{m,m+1}\langle m+1|, \end{aligned} \tag{1}$$

where $\mathcal{H}$ is the effective Hamiltonian describing the coupled-resonator system, ω_l is the lth eigenfrequency of the SSH chain and $\psi_m^{(l)}$ represents the corresponding magnetic field amplitude of the lth supermode in the individual resonator (Wannier) basis $|m\rangle$ localized at the $\{m = [-(N-1)/2]\cdots[(N-1)/2]\}$th resonator (site) [37]. In this representation, the Wannier modes $|m\rangle$ correspond to the magnetic field of the first transverse electric mode that is perpendicular to the metallic top and bottom plates [32]. The resonant frequency of the mth resonator is indicated as $\epsilon_m = \epsilon$ (for $m \neq 0$) and $t_{m,m+1}$ is the coupling coefficient between mth and $(m+1)$th resonators [37]. The defect resonator is at position $m \equiv m_D = 0$ at the center of the array (see Fig. 1). Hamiltonian (1) (in the absence of nonlinearities and $N \to \infty$) has a band structure with $\omega(k) = \epsilon \pm \sqrt{t_1^2 + t_2^2 + 2t_1 t_2 \cos(k)}$ ($k \in [-\pi;\pi]$ is the wave number) and one defect mode at $\omega_D = \epsilon$ (center of the gap). The nonlinearity due to the presence of the PIN diode has been incorporated in Eq. (1) by modifying the resonant frequency ϵ_D as

$$\epsilon_D = \epsilon + \Omega(I_D), \tag{2}$$

where $\Omega(I_D)$ is a nonlinear function of the local field intensity $I_D = |\psi_D|^2$ at m_D. The pure linear chain of coupled resonators with nearest neighbor couplings has a chiral symmetry where the chiral symmetric operator $\mathcal{C}$, written in the Wannier basis as $\langle m_1|\mathcal{C}|m_2\rangle = (-1)^{m_1}\delta_{m_1,m_2}$. A similar experimental setup has been used to investigate the Gaussian chiral symmetry classes [38]. If complex eigenfrequencies are present, i.e., losses, then the time-reversal operator $\mathcal{T}$ (complex conjugation) does not commute with $\mathcal{H}$. In case where $\Omega(I_D)$ is purely imaginary, the system respects a $\mathcal{CT}$ symmetry, defined as anticommutation of the Hamiltonian $\mathcal{H}$ with the $\mathcal{CT}$ operator. Charge conjugation symmetry imposes restrictions to the spectrum of the system; namely eigenstates of a $\mathcal{CT}$-symmetric Hamiltonian $\mathcal{H}$ come in pairs as $\mathcal{CT}$-symmetric partners. In particular, given an eigenstate $\mathcal{H}|\Psi\rangle = \omega|\Psi\rangle$ the $\mathcal{CT}$ partner is $\mathcal{HCT}|\Psi\rangle = -\omega^*\mathcal{CT}|\Psi\rangle$. Thus the spectrum of $\mathcal{H}$ is mirror symmetric with respect to the resonant frequency of the individual resonators. An eigenstate whose $\mathcal{CT}$ partner is distinct from itself is referred to be in broken $\mathcal{CT}$-symmetric phase, whereas an eigenstate in the exact $\mathcal{CT}$-symmetric phase is the $\mathcal{CT}$ symmetric partner of itself, $\mathcal{CT}|\Psi\rangle = |\Psi\rangle$. It follows that an exact $\mathcal{CT}$-symmetric state has purely imaginary eigenfrequency shift, i.e., $\mathrm{Re}(\omega) - \epsilon = 0$. Moreover, a global complex phase in the wave function of such a state can be chosen such that purely real (imaginary) components occupy the even- (odd-) numbered sublattices [39]. For more details on $\mathcal{CT}$ operator in coupled mode theory refer to [40].

Theoretical analysis of defect mode.—To investigate the symmetry-induced topological features of the defect mode we developed a non-Hermitian nonlinear Green's function formalism. We decompose the total Hamiltonian $\mathcal{H}$ into an unperturbed Hermitian $\mathcal{H}_0$ and a non-Hermitian perturbation $\mathcal{H}_1$ which describes the lossy nonlinearity at site m_D. Specifically

$$\mathcal{H} = \mathcal{H}_0 + \mathcal{H}_1; \quad \mathcal{H}_1 = |D\rangle\Omega(I_D)\langle D|, \tag{3}$$

where $|D\rangle$ indicates the Wannier state at the defect site. The Green's function $\mathcal{G}(z) \equiv (z-\mathcal{H})^{-1}$ of the total Hamiltonian reads [41,42]

$$\begin{aligned}\mathcal{G}(z) &= \mathcal{G}_0(1-\mathcal{H}_1\mathcal{G}_0)^{-1},\\ &= \mathcal{G}_0[1+\mathcal{H}_1\mathcal{G}_0+(\mathcal{H}_1\mathcal{G}_0)^2+\cdots],\\ &= \mathcal{G}_0+\mathcal{G}_0\mathcal{T}\mathcal{G}_0,\end{aligned} \tag{4}$$

where $\mathcal{G}_0(z) \equiv (z-\mathcal{H}_0)^{-1}$ is the Green's function of $\mathcal{H}_0$ and $\mathcal{T}(z) = |D\rangle[\Omega/(1-\langle D|\mathcal{G}_0|D\rangle\Omega)]\langle D|$ is the t matrix [41]. From the last line of Eq. (4) we can evaluate the simple pole $z=\omega_D$ of $\mathcal{G}$ corresponding to the eigenfrequency of the defect state. The latter is the solution of

$$\langle D|\mathcal{G}_0(\omega_D)|D\rangle = \Omega(I_D)^{-1}, \tag{5}$$

while the corresponding residue is

$$\mathrm{Res}[\langle D|\mathcal{G}(z)|D\rangle]_{z=\omega_D} = \frac{(\psi_D^{(D)})^2}{\chi} = \left[-\frac{\langle D|\mathcal{G}_0|D\rangle^2}{\frac{d\langle D|\mathcal{G}_0|D\rangle}{dz}}\right]_{z=\omega_D}, \tag{6}$$

where $\psi_D^{(D)}$ is the 0th component of the defect eigenstate (in the Wannier basis, $m_D=0$).. As opposed to Hermitian defect perturbation methods [41,42], the first equality in Eq. (6) requires to use the fact that in non-Hermitian systems the eigenmodes are biorthogonal, i.e., $\sum_l[(|\Psi_l\rangle\langle\Phi_l|)/(\langle\Phi_l|\Psi_l\rangle)] = \mathbb{1}$, where $|\Psi_l\rangle$ and $\langle\Phi_l|$ denote the lth right and left eigenvectors of $\mathcal{H}$, respectively. In case of non-Hermitian systems, the eigenvectors are normalized as $\langle\Phi_l|\Psi_{l'}\rangle = \sum_m \psi_m^{(l)}\psi_m^{(l')} = \chi\delta_{l,l'}$ where we have used the fact that $|\Psi_l\rangle = (|\Phi_l\rangle)^*$ in case of symmetric non-Hermitian Hamiltonians $\mathcal{H} = \mathcal{H}^T$. χ is the so-called quasipower whose analog in Hermitian physics is the total power of the signal [43]. Equations (5) and (6) are solved self-consistently for ω_D and $\psi_D^{(D)}$ using various quasipower values χ which is a free parameter. Using Eq. (6) we evaluate $\psi_D^{(D)}$ as a function of χ and the injected power $I_D \equiv |\psi_D^{(D)}|^2$ which is further compared to the experimental value P_{VNA}. This comparison identifies the appropriate quasipower χ associated with the experimental incident power. All components of the defect mode $\psi_m^{(D)}$ can be evaluated from Eq. (4) using the same steps. We have

$$\frac{(\psi_m^{(D)})^2}{\chi} = \left[-\frac{\langle m|\mathcal{G}_0|D\rangle\langle D|\mathcal{G}_0|m\rangle}{\frac{d\langle D|\mathcal{G}_0|D\rangle}{dz}}\right]_{z=\omega_D}. \tag{7}$$

Knowledge of ω_D and of the corresponding field amplitudes $\{\psi_m^{(D)}\}$ allows us to construct any other physical observable. One is the field intensity $I_D \equiv |\psi_D|^2$ at site $m_D = 0$, which is associated with the pump power and it is the controlled variable in the pump-probe experiment of Fig. 1. In the specific case of the SSH with a lossy nonlinear defect, Eqs. (5)–(7) have been solved numerically by calculating the unperturbed Green's function $\mathcal{G}_0$ with system size $N=17$. The theoretical results have been then compared with the experimental findings. An alternative derivation is provided in [44] based on an ansatz for the form of the defect mode.

Results—An analysis of the experimental transmission spectrum of the SSH array including a defect resonator with a diode and a comparison with the theoretical analysis of the spectrum allowed us to extract the nonlinear term $\Omega(I_D)$ appearing in Eq. (2). The best fit occurs for the expression:

$$\Omega(I_D) = \Omega_{\mathrm{sat}}(I_D) = z_0 - \frac{z_1}{1+\alpha I_D}, \tag{8}$$

where $z_0 = (-40+18\imath)$ MHz, $z_1 = (-40+8\imath)$ MHz, $\alpha = (1-2.8\imath)$ mW^{-1} have been extracted via comparison between the measured values of the defect frequency (see below) and the theoretical predictions (we have assumed that $\alpha_{\mathrm{lin}} = 1$, i.e., $I_D = P_{\mathrm{VNA}}$). This equation describes a saturable absorption and is applicable for all powers used in our experiments.

For moderate values of the pump power up to $I_D \approx -10$ dBm the nonlinearity can be described by

$$\Omega(I_D) \approx \Omega_{\mathrm{tpa}}(I_D) = (\beta_0 + \beta_1 I_D). \tag{9}$$

Such nonlinearity has its own merit—specifically in optical range—where it describes a two-photon absorption (TPA) nonlinear mechanism. As we will see below it conserves the $\mathcal{CT}$ symmetry of the effective Hamiltonian Eq. (1) (i.e., the Hamiltonian anticommutes all the time with the $\mathcal{CT}$ operator) and therefore deserves a separate study by itself. In this pump power regime, one can safely assume that $\beta_0 \equiv (z_0 - z_1) = 10i$ MHz and $\beta_1 \equiv z_1\alpha = (17.6 + 120i)$ MHz/mW has a negligible real part [$\mathrm{Re}[z_1\alpha] \approx -17.6$ MHz/mW $\ll \epsilon/I_D \approx 6.876$ GHz/$(-10$ dBm$) = 68\,760$ MHz/mW] and therefore can be considered to be imaginary. Therefore, the system respects the $\mathcal{CT}$ symmetry, while preserving the band gap; thus offering a topological protection to the defect mode as discussed in linear systems [16].

We first present the parametric evolution of the defect frequency ω_D versus the pump power P_{VNA}, see Fig. 2. The experimental values for ω_D (filled circles) have been extracted from the measured transmission spectra. A resonance peak in the middle of the band gap signifies the presence of the defect mode, and we have recorded the trace of such peak with increasing pump power. Additionally, we present in Fig. 2 the theoretical results for the defect frequency, extracted from the analysis of Eqs. (5) and (6) using the nonlinear form Eq. (8). For $P_{\mathrm{VNA}} \leq -10$ dBm the TPA form of $\Omega(I_D)$ [Eq. (9)]

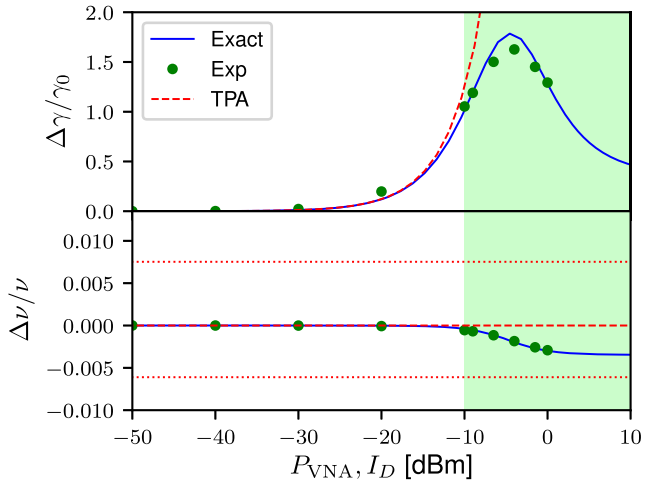

FIG. 2. Spectral shift of the complex defect mode frequency $\omega_D = \nu_D + i\gamma_D$ with varying injected power P_{VNA} (expressed as dBm) at the defect site. Note that shifts in the real and imaginary parts of the eigenfrequency have each been renormalized with respect to its low P_{VNA} limit, ν_0 and γ_0, respectively. Measurements (green dots) of the eigenfrequency show agreement with the theoretical results (blue curves), with $\Omega(I_D)$ given by the first expression in Eq. (8). Up to moderate P_{VNA}, the experimentally found nonlinearity can be well described by Eq. (9) (TPA), from which we have also calculated the complex eigenfrequency (red dashed curves). The red dotted lines signify the upper and lower limits of the band gap, extracted from the measured transmission spectra.

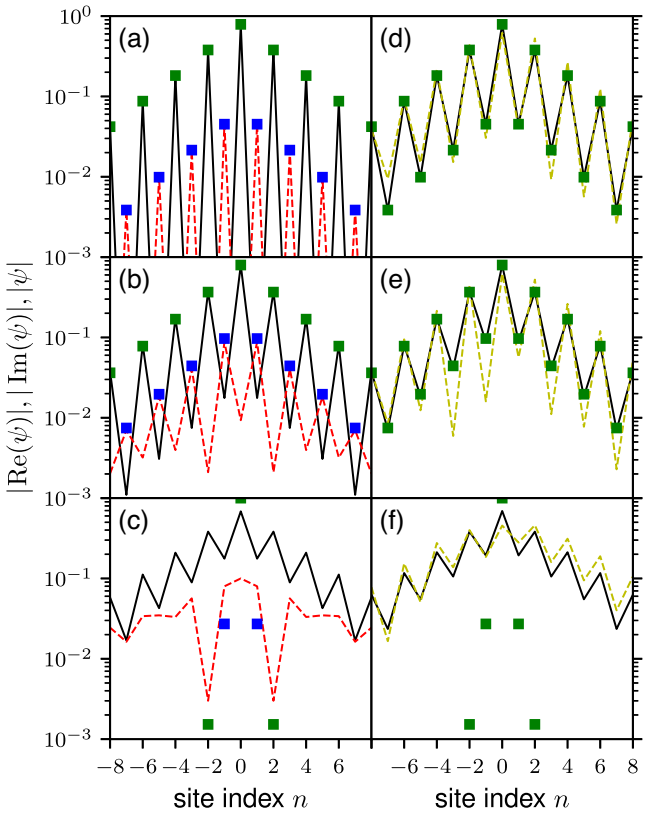

FIG. 3. (Left column) Theoretical calculations for the $\mathrm{Re}(\psi_m^{(D)})[\mathrm{Im}(\psi_m^{(D)})]$ using the saturable absorption, Eq. (8) (black line [red dashed line]), and the two-photon absorption, Eq. (9) (green [blue] squares), expression for $\Omega(I_D)$ for three pumping powers P_{VNA} (a) -40 dBm, (b) -10 dBm, (c) 10 dBm. Right column: experimental modulus profiles $|\psi_m^{(D)}|$ (yellow dashed lines) for three pumping powers P_{VNA} (d) -40 dBm, (e) -10 dBm, and (f) 10 dBm. The theoretical calculations using the saturable [Eq. (8)] or TPA [Eq. (9)] form for the nonlinearity are also reported with black solid lines or green squares. In all cases the presented wave functions are normalized setting $(\sum_m |\psi_m|^2 = 1)$.

captures all features of the experimental data and consequently the defect frequency $\nu_D = \mathrm{Re}(\omega_D)$ is pinned to ν_0, while its imaginary part $\gamma_D = \mathcal{I}m(\omega_D)$ significantly grows with the pump power I_D due to the corresponding increase in the amount of nonlinear loss. Hence, the $\mathcal{CT}$ symmetry enforces a spectral (topological) protection against self-induced variations of the resonant frequency of the defect resonator. For even higher values of the pump power P_{VNA} (highlighted area in Fig. 2) the TPA expression for the nonlinearity Eq. (9) is not sufficient to describe the experimental results. Instead Eq. (8) adequately describes the real (nonlinear) frequency shift of the defect resonator, thus enforcing an explicit (self-induced) violation of the $\mathcal{CT}$ symmetry. Indeed, when $\mathrm{Re}(\epsilon_d) \to \epsilon + \mathrm{Re}[\Omega(I)]$, with $\mathrm{Re}[\Omega(I)] \neq 0$, one can show that $\{H, \mathcal{CT}\} \neq 0$, i.e., the effective Hamiltonian (1) does not respect the $\mathcal{CT}$ symmetry. Consequently, when $P_{\mathrm{VNA}} \geq -10$ dBm the defect frequency ν_D is not protected but rather shifts towards the band [45].

Next, we investigate the field profiles of the defect mode for various pump powers P_{VNA}. In Fig. 3(left) we report the theoretical calculation of the field amplitudes $\psi_m^{(D)}$ for three representative values of $P_{\mathrm{VNA}} = -40$ dBm, -10 dBm, and 10 dBm. We find that for pump powers $P_{\mathrm{VNA}} \leq -10$ dBm, the defect mode respects the $\mathcal{CT}$ symmetry as it is evident from the fact that all even (odd) sites are occupied by purely real (imaginary) wave function components. This analysis reconfirms our previous conclusion, which was based on the ν_D vs P_{VNA} analysis: as long as the nonlinearity can be described by the TPA expression [Eq. (9)] (i.e., it is purely imaginary), the defect mode is in the so-called *exact* $\mathcal{CT}$-symmetric phase (i.e., it is also an eigenmode of the $\mathcal{CT}$ operator). In contrast, for higher pump powers [see Fig. 3(c)] the $\Omega(I_D)$ develops a considerable real part and the system experiences a self-induced $\mathcal{CT}$-symmetry violation. This is reflected in the fact that the real and imaginary parts of $\psi_m^{(D)}$ do not have any more a staggered form; i.e., $\psi_m^{(D)}$ is not an eigenstate of $\mathcal{CT}$ operator (broken phase).

The validity of the theoretical analysis of the field profile has been accessed via a direct comparison with the experimental measurements of the defect modulus profile

$|\psi_m^{(D)}|$, see Fig. 3 (right). The resulting agreement between the TPA form of $\Omega(I_D)$ and the "actual" form is impressive for pump powers $P_{\mathrm{VNA}} \leq -10$ dB ms. This indicates that up to this pump power the system (effectively) respects the $\mathcal{CT}$ symmetry [see Figs. 3(a) and 3(b)] and is in good agreement with the experiment [see Figs. 3(d) and 3(e)]. Above −10 dBm, the two forms of the nonlinearity provide different results indicating that the system has entered the self-induced explicit $\mathcal{CT}$-symmetric violation regime. Nevertheless, our theoretical calculations using the exact form of $\Omega(I_D)$ still agree nicely with the experimentally extracted wave profile [see Figs. 3(c) and 3(f)].

Conclusions.—We have analyzed and demonstrated the topological properties of a nonlinear $\mathcal{CT}$-symmetric defect mode both theoretically and experimentally using a microwave platform that realizes a SSH CRMW array with a defect resonator coupled inductively to a PIN diode. When the diode-induced nonlinearity is purely imaginary, the nonlinear defect mode is spectrally protected by the non-Hermitian $\mathcal{CT}$ symmetry. In particular, the defect frequency is in the middle of the band gap while the field amplitude of the defect mode has a characteristic shape involving staggered imaginary and real parts. For high pump powers, the nonlinearity acquires a sizable real part and the system experiences a self-induced explicit symmetry violation. In this case the defect mode is not any more protected by the $\mathcal{CT}$ symmetry. The self-induced $\mathcal{CT}$-symmetry violation can be an extremely desirable feature for various technological applications of topological photonics varying from topological protection of unidirectional defect modes at low incident powers to photonic reflective limiters.

T. K. and D. H. J. acknowledge partial support from Grant No. ONR N00014-19-1-2480, from AFOSR via MURI Grant No. FA9550-14-1-0037 and from Grant No. NSF EFMA-1641109.

*fabrice.mortessagne@univ-cotedazur.fr
†tkottos@wesleyan.edu
‡ulrich.kuhl@univ-cotedazur.fr

[1] L. Lu, J. D. Joannopoulos, and M. Soljačić, Topological photonics, Nat. Photonics **8**, 821 (2014).
[2] T. Ozawa, H. M. Price, A. Amo, N. Goldman, M. Hafezi, L. Lu, M. C. Rechtsman, D. Schuster, J. Simon, O. Zilberberg, and I. Carusotto, Topological photonics, Rev. Mod. Phys. **91**, 015006 (2019).
[3] F. D. M. Haldane and S. Raghu, Possible Realization of Directional Optical Waveguides in Photonic Crystals with Broken Time-Reversal Symmetry, Phys. Rev. Lett. **100**, 013904 (2008).
[4] Z. Wang, Y. Chong, J. D. Joannopoulos, and M. Soljačić, Observation of unidirectional backscattering-immune topological electromagnetic states, Nature (London) **461**, 772 (2009).
[5] M. C. Rechtsman, J. M. Zeuner, Y. Plotnik, Y. Lumer, D. Podolsky, F. Dreisow, S. Nolte, M. Segev, and A. Szameit, Photonic Floquet topological insulators, Nature (London) **496**, 196 (2013).
[6] M. Hafezi, S. Mittal, J. Fan, A. Migdall, and J. M. Taylor, Imaging topological edge states in silicon photonics, Nat. Photonics **7**, 1001 (2013).
[7] Y. Hadad, V. Vitelli, and A. Alu, Solitons and propagating domain walls in optical resonator arrays, ACS Photonics **4**, 1974 (2017).
[8] Y. Lumer, Y. Plotnik, M. C. Rechtsman, and M. Segev, Self-Localized States in Photonic Topological Insulators, Phys. Rev. Lett. **111**, 243905 (2013).
[9] D. Leykam and Y. D. Chong, Edge Solitons in Nonlinear Photonic Topological Insulators, Phys. Rev. Lett. **117**, 143901 (2016).
[10] Y. Wang, L.-J. Lang, C. H. Lee, B. Zhang, and Y. D. Chong, Topologically enhanced harmonic generation in a nonlinear transmission line metamaterial, Nat. Commun. **10**, 1102 (2019).
[11] X. Zhu, Y. Wang, D. Leykam, and Y. D. Chong, Optical isolation with nonlinear topological photonics, New J. Phys. **19**, 095002 (2017).
[12] S. Malzard, E. Cancellieri, and H. Schomerus, Topological dynamics and excitations in lasers and condensates with saturable gain or loss, Opt. Express **26**, 22506 (2018).
[13] Y. Hadad, A. B. Khanikaev, and A. Alu, Self-induced topological transitions and edge states supported by nonlinear staggered potentials, Phys. Rev. B **93**, 155112 (2016).
[14] Y. Hadad, J. C. Soric, A. B. Khanikaev, and A. Alú, Self-induced topological protection in nonlinear circuit arrays, National electronics review **1**, 178 (2018).
[15] D. A. Dobrykh, A. V. Yulin, A. P. Slobozhanyuk, A. N. Poddubny, and Y. S. Kivshar, Nonlinear Control of Electromagnetic Topological Edge States, Phys. Rev. Lett. **121**, 163901 (2018).
[16] H. Schomerus, Topologically protected midgap states in complex photonic lattices, Opt. Lett. **38**, 1912 (2013).
[17] J. M. Zeuner, M. C. Rechtsman, Y. Plotnik, Y. Lumer, S. Nolte, M. S. Rudner, M. Segev, and A. Szameit, Observation of a Topological Transition in the Bulk of a Non-Hermitian System, Phys. Rev. Lett. **115**, 040402 (2015).
[18] C. Poli, M. Bellec, U. Kuhl, F. Mortessagne, and H. Schomerus, Selective enhancement of topologically induced interface states in a dielectric resonator chain, Nat. Commun. **6**, 6710 (2015).
[19] S. Weimann, M. Kremer, Y. Plotnik, Y. Lumer, S. Nolte, K. G. Makris, M. Segev, M. C. Rechtsman, and A. Szameit, Topologically protected bound states in photonic parity-time-symmetric crystals, Nat. Mater. **16**, 433 (2017).
[20] T. E. Lee, Anomalous Edge State in a Non-Hermitian Lattice, Phys. Rev. Lett. **116**, 133903 (2016).
[21] D. Leykam, K. Y. Bliokh, C. Huang, Y. D. Chong, and F. Nori, Edge Modes, Degeneracies, and Topological Numbers in Non-Hermitian Systems, Phys. Rev. Lett. **118**, 040401 (2017).
[22] U. Kuhl, F. Mortessagne, E. Makri, I. Vitebskiy, and T. Kottos, Waveguide photonic limiters based on topologically protected resonant modes, Phys. Rev. B **95**, 121409(R) (2017).

[23] E. Makri, R. Thomas, and T. Kottos, Reflective limiters based on self-induced violation of $\mathcal{CT}$ symmetry, Phys. Rev. A **97**, 043864 (2018).
[24] H. Shen, B. Zhen, and L. Fu, Topological Band Theory for Non-Hermitian Hamiltonians, Phys. Rev. Lett. **120**, 146402 (2018).
[25] V. M. M. Alvarez, J. E. B. Vargas, M. Berdakin, and L. E. F. F. Torres, Topological states of non-Hermitian systems, Eur. Phys. J. Spec. Top. **227**, 1295 (2018).
[26] G. Harari, M. A. Bandres, Y. Lumer, M. C. Rechtsman, Y. D. Chong, M. Khajavikhan, D. N. Christodoulides, and M. Segev, Topological insulator laser: Theory, Science **359**, eaar4003 (2018).
[27] M. A. Bandres, S. Wittek, G. Harari, M. Parto, J. Ren, M. Segev, D. N. Christodoulides, and M. Khajavikhan, Topological insulator laser: Experiments, Science **359**, eaar4005 (2018).
[28] H. Zhao, P. Miao, M. H. Teimourpour, S. Malzard, R. El-Ganainy, H. Schomerus, and L. Feng, Topological hybrid silicon microlasers, Nat. Commun. **9**, 981 (2018).
[29] Z. Gong, Y. Ashida, K. Kawabata, K. Takasan, S. Higashikawa, and M. Ueda, Topological Phases of Non-Hermitian Systems, Phys. Rev. X **8**, 031079 (2018).
[30] M. Segev and M. A. Bandres, Viewpoint: Non-Hermitian topological systems, Physics **11**, 96 (2018).
[31] K. Kawabata, K. Shiozaki, M. Ueda, and M. Sato, Symmetry and Topology in Non-Hermitian Physics, Phys. Rev. X **9**, 041015 (2019).
[32] M. Reisner, F. Mortessagne, E. Makri, T. Kottos, and U. Kuhl, Microwave limiters implemented by coupled dielectric resonators based on a topological defect mode and CT-symmetry breaking, Acta Phys. Pol. A **136**, 790 (2019).
[33] M. Reisner, D. H. Jeon, C. Schindler, H. Schomerus, F. Mortessagne, U. Kuhl, and T. Kottos, Self-Shielded Topological Receiver Protectors, Phys. Rev. Appl. **13**, 034067 (2020).
[34] W. P. Su, J. Schrieffer, and A. J. Heeger, Solitons in Polyacetylene, Phys. Rev. Lett. **42**, 1698 (1979).
[35] H. A. Haus and W. Huang, Coupled-mode theory, Proc. IEEE **79**, 1505 (1991).
[36] A. Barybin and V. Dmitriev, *Modern Electrodynamics and Coupled-Mode Theory: Application to Guided-Wave Optics*, 1st ed. (Rinton Press, Inc., Princeton, New Jersey, 2002).
[37] M. Bellec, U. Kuhl, G. Montambaux, and F. Mortessagne, Tight-binding couplings in microwave artificial graphene, Phys. Rev. B **88**, 115437 (2013).
[38] A. Rehemanjiang, M. Richter, U. Kuhl, and H.-J. Stöckmann, Microwave Realization of the Chiral Orthogonal, Unitary, and Symplectic Ensembles, Phys. Rev. Lett. **124**, 116801 (2020).
[39] In the special case where $\Omega(I_D)$ is negligible, the Hamiltonian respects chiral symmetry; i.e., the Hamiltonian $\mathcal{H}$ anticommutes with the $\mathcal{C}$ operator. Chiral symmetric states ($\mathcal{C}|\Psi\rangle = |\Psi\rangle$) have fixed eigenvalues at zero ($\omega = 0$), and their mode profiles show a characteristic staggered shape ($\psi_m = 0$ for all odd m).
[40] S. Malzard, C. Poli, and H. Schomerus, Topologically Protected Defect States in Open Photonic Systems with Non-Hermitian Charge-Conjugation and Parity-Time Symmetry, Phys. Rev. Lett. **115**, 200402 (2015).
[41] E. N. Economou, *Green's Functions in Quantum Physics*, Springer Series in Solid State Sciences Vol. 7 (Springer-Verlag, Berlin, 1974).
[42] M. I. Molina and G. P. Tsironis, Nonlinear impurities in a linear chain, Phys. Rev. B **47**, 15330 (1993).
[43] K. G. Makris, R. El-Ganainy, D. N. Christodoulides, and Z. H. Musslimani, Beam Dynamics in pt-Symmetric Optical Lattices, Phys. Rev. Lett. **100**, 103904 (2008).
[44] See the Supplemental Material at http://link.aps.org/supplemental/10.1103/PhysRevLett.125.113901 for details the Non-Hermitian Green's Function and describes an alternative method (the ansatz method) to evaluating the defect mode.
[45] A more refined phase-diagram of pump frequency vs pump power is experimentally challenging due to weak nonlinear effects away from resonant frequency. In this respect, our results shown in Fig. 2 are at a pump frequency that is at resonant, thus constituting a lower intensity bound for which $\mathcal{CT}$ symmetry is violated.